Commercial NHL-containing mortars for the preservation of historical architecture. Part 2: Durability to salt decay

Davide Gulotta [a,*], Sara Goidanich [a], Cristina Tedeschi [b], Lucia Toniolo [a]

[a] *Politecnico di Milano – Dipartimento di Chimica, Materiali e Ingegneria Chimica "Giulio Natta", Via Mancinelli 7, 20131 Milano, Italy*
[b] *Politecnico di Milano – Dipartimento di Ingegneria Civile e Ambientale, Piazza L. Da Vinci 32, 20133 Milano, Italy*

Received 4 August 2014
Received in revised form 16 July 2015
Accepted 4 August 2015
Available online 10 August 2015

1. Introduction

Salt crystallization within the porous matrix of the architectural materials has been recognised as a major and widespread cause of decay since a long time [1]. Salt weathering of the built heritage is ubiquitous and case studies involving various construction materials and techniques, as well as occurring in rather different environmental conditions, have been extensively reported in the scientific literature [2–6]. The relevance and complexity of this decay mechanism with respect to the conservation of the architectural heritage, as well as the related issues which still remain not completely solved, have been summarised by several authors in recent years [7–10]. The extent of salt weathering is mainly related to the diffusion and availability of a number of possible salt sources in both urban and rural environments. These include atmospheric pollutants (in particular sulphates and nitrates), marine aerosols, deicing products, rising damp from contaminated soils, chemical

* Corresponding author.
E-mail addresses: davide.gulotta@polimi.it (D. Gulotta), sara.goidanich@polimi.it (S. Goidanich), cristina.tedeschi@polimi.it (C. Tedeschi), lucia.toniolo@polimi.it (L. Toniolo).

interaction of building materials [8]. Significant amount of soluble salts may also derive from the construction materials themselves [11] or as a result of not compatible conservative treatments [12]. Once saline solutions penetrate inside the porous matrix, or salts form directly within the material, cycles of crystallization/dissolution take place as a result of the variations of environmental conditions, namely temperature, relative humidity and air speed. According to the duration and magnitude of such variations, as well as to the specific solubility of the single salt involved (or mix-tures of salts [13]), saline solutions tend either to migrate through the porosity deep in the bulk of the material or to accumulate near the surface [14]. The presence of moisture can therefore be consid-ered as an essential catalyst for salt-induced damage to occur [15], as it both plays a role during the contamination phase and it strongly influences the migration of the saline solutions, thus determining the crystallization location. As far as this last param-eter is concerned, it is worth noting that not all crystallization phenomena will result in damage of the material. Efflorescences and formation of superficial salt crusts are deterioration patterns frequently observed on the surface of salt loaded substrates. These crystallization forms are not usually associated to relevant damages of the porous matrixes, even though they can increase the amount of superficial moisture due to salt hygroscopicity and they also have a remarkable impact under the aesthetic point of view. On the contrary, crystal growth in the bulk or just below the surface evaporation front actually represents a far more dangerous scenario.

As far as the historic masonries are concerned, salt crystallization can be particularly critical for the mortars used for the bedding of blocks and bricks, as it can lead to the loss of construction elements thus compromising the structural function-ality. The damage progression has to be counteracted by restoring the integrity of the overall masonry system and requires the use of repair mortars. The most appropriate mortar recipe for such operations should be defined taking into account the specific characteristics of the substrate and of the original mortars, as well as their state of conservation, and the environmental conditions. Moreover, the mortar should be designed in order to match as close as possible the historic one to be replaced/integrated. This approach is widely recognised as a "good practice" and it is pur-sued in a number of practical guidelines and protocols [16–18] in order to ensure the overall compatibility of the intervention [19–22]. On the other hand, the traditional on-site preparation of the mortars starting from the anhydrous raw materials can be highly time-consuming and, in some cases, hardly sustainable under an economic point of view. Commercial ready-mixed mortars based on natural hydraulic limes (NHL) can provide an advantageous alternative to the traditionally prepared ones.

In a recent paper [23], a selection of the most diffused commercial products (two NHL binders and four NHL-based commercial ready-mixed mortars) was characterised. As a consequent step, the present study aims at investigating the durability of hardened mortars prepared with the same commercial materials with respect to salt crystallization. The salt resistance of traditionally prepared repair mortars has been extensively studied both on site and in laboratory conditions [24,25]. On the other hand, the durability of commercial ready-mixed mortars has been scarcely investigated so far, despite their increasing use. A wide number of different testing methodologies has been proposed, involving different saline solutions, salt contamination procedures, type of substrates, test durations, etc., as recently summarised by Arizzi et al. [24]. In the case of bedding mortars, salt crystallization tests allow to identify the main decay patterns and to evaluate the damage extent rapidly, by keeping the most effective test conditions in order to promote fast and intense damage evolution. However, the great number of concurrent environmental parameters acting in real environments, as well as the heterogeneity of historic masonries, can hardly be reproduced in the lab. Therefore, the reliability of the laboratory results with respect to the effective long-term on site behaviour of the tested materials is still debated [8].

For the present study, the RILEM test for the determination of the resistance of mortars and simplified masonry systems (wallettes) to sulphates and chlorides has been used [26]. In particular, sodium sulphate solutions have been used according to the well-known activity of this salt, which is therefore widely employed to test the sulphate resistance of porous materials [24–27]. Sodium sulphate can crystallize in three differently hydrated phases: thenardite (NA_2SO_4), mirabilite ($NA_2SO_4{\cdot}10H_2O$), and a metastable heptahydrate phase ($NA_2SO_4{\cdot}7H_2O$) [27,28]. At room temperature (T = 20 °C) the phase transition between thenardite and mirabilite occurs around a relative humidity (RH) of 75%, and the equilibrium humidity of a saturated mirabilite solution is around 93%. Stability of mirabilite is strongly temperature-dependent, it decreases as the temperature rises and this phase do not crystallize above 32 °C. The extensive damaging of porous materials contaminated by sodium sulphate solutions is related to the high crystallization pressure that is generated, which can locally overcome the tensile strength of the substrate. In order to cause damage, the stress field induced by crystallization has to be large enough to propagate critical flaws in the material [29]. Crystallization pressure depends on the degree of supersaturation of the solution, and can reach high values for mirabilite growth. Highly supersaturated mirabilite formation is reported after disso-lution of thenardite crystals inside a porous matrix (i.e., as a result of RH increasing) [30]. Mirabilite is therefore generally considered as the most effective damaging phase [29], but this particular aspect of the deterioration mechanism is still under study [30]. More recently, also the metastable heptahydrate phase has been identified as playing a major role in the damage mechanism. This phase may in fact be the first one forming upon cooling a porous system saturated by a sodium sulphate solution [31].

RILEM test conditions are defined in order to promote mirabilite formation. In particular, environmental T and RH values are kept steady during the entire procedure so that the evaporation rate of the sodium sulphate solution favours mirabilite crystallization just beneath the surface of the tested materials. In such way the damage is maximised. Durability of commercial products has been here preliminary studied on mortar specimens and then a 12 months-long test has been conducted on masonry wallettes. The damage evolution has been continuously monitored by means of visual and microscopical observation; the damage extent has been evaluated as loss of material and through scanning laser profilometry. The overall durability of commercial mortars has been studied with respect to the evolution of the deterioration patterns. The characterisation and durability results have been treated by means of Principal Component Analysis (PCA), which has been used for classification, provenance and deterioration studies of his-toric mortars [32,33], and it is here applied to the investigation of the factors which mostly affect the decay. PCA allows reducing the dimensionality of the initial data by calculating a new set of variable (principal components – PC) which are linear combinations of the original ones. The PCs still retain all the relevant information and can be represented graphically in order to emphasise the data correlation.

2. Materials and methods

2.1. Products and suppliers

A selection of four NHL-based ready-mixed commercial mortars (named M1–M4) and two NHL commercial binders (named B1 and B2) was made among the most diffused products available in the market [23]. According to the current

standard [34] M3 and B1 are classified as NHL 3.5; M4 and B2 are classified as NHL 5; compressive strength classes of M1 and M2 are not indicated. Binders B1 and B2 were mixed with standard quartz-siliceous sand for the mortars preparation.

Wallettes were prepared with traditional fire-clayed red bricks, type "San Marco" (San Marco, Italy).

2.2. Specimen preparation

Mortars were prepared following the technical indications of the suppliers and standard recommendations [35]. B1 and B2 binders were mixed with standard aggregate (standard quartz-siliceous sand with controlled granulometry and constant mineralogical composition) and water. The proportions by mass were 1:3:0.5 (binder:aggregate:water). Ready-mixed mortars powders were just mixed with the required amount of clean water. All mixing operations were performed with a mechanical mortar mixer according to European technical standard in controlled conditions [35].

Two types of specimen were prepared: (a) standard $4 \times 4 \times 16$ cm mortar prismatic specimens casted in demountable steel mould and compacted by mechanical vibration; (b) 25×24 cm wallettes made of three courses of bricks (two entire units and a half-divided one) so that two horizontal joints of mortars and a vertical one are obtained. The thickness of mortar joints is around 2.5 cm.

Specimens of both sets were stored at 20 °C-90% RH for 60 days. At the end of the curing time, the prismatic mortar specimens were divided into 4 cm cubic unit by means of a precision cutting diamond wheel.

2.3. Crystallization tests

Crystallization tests on two sets of cubic mortar specimen were performed according to a modified version of RILEM MS-A.2 procedure [26]. Specimens were sealed along the four lateral faces and dried at 60 °C until constant weight. Salt contamination was performed with a 10% sodium sulphate solution (anhydrous Na_2SO_4 reagent grade, Fluka) in which the specimens were immersed to a 1 cm depth for 2 h. The imbibition phase was followed by a 22 h drying period at 20 °C–80% RH. Daily cycles (2 h imbibition + 22 h drying) were repeated 4 times a week (week-cycle). After each week-cycle specimens were dried at 60 °C and those belonging to set 1 alone were brushed to remove all the efflorescences and the debris resulting from crystallization. Mass variation was then recorded to obtain the damage extent as loss of material (set 1) and the salt uptake over time (set 2). The initial weight (M_i) of the unaltered specimens was normalised to 100%; the final one (M_f) at the end of the test was normalised accordingly ($M_{f\%} = M_f/M_i * 100$). Cycles have been repeated until a significant damage was caused to most of the specimens.

Testing of wallettes has been performed strictly according to the RILEM MS-A.1 procedure [26]. Wallettes have been subjected to an initial capillary imbibition with a 10% Na_2SO_4 saline solution which provided the unique source of salt during the entire test. Dissolution and re-crystallization has been then promoted at the end of each 4 weeks cycle by adding water to the system. The test conditions have been steadily kept at 20 °C and 50% RH avoiding fast evaporation and drying of the specimens. These conditions are stable for thenardite precipitation on the upper evaporation surface of the specimens exposed to the external environment, whereas in a thin region of the material just beneath it mirabilite formation is promoted [26]. Ten crystallization cycles were carried out over a 12 months testing period.

2.4. Analytical techniques

2.4.1. Stereomicroscopy

The damage evolution and decay patterns were observed by means of a Leica M205C stereomicroscope, equipped with a Leica DFC290 digital camera.

2.4.2. Fourier transformed infrared spectroscopy (FTIR)

FTIR spectroscopy was carried out by a Thermo Nicolet 6700 instrument using a DTGS detector in the spectral range 4000–400 cm^{-1} with 4 cm^{-1} resolution. Fine grinded samples of efflorescences were analysed in transmission mode after dispersion in KBr pellets.

2.4.3. X-ray diffraction (XRD)

The mineralogical phases of ready mixed mortars and binders were investigated by a Philips PW1830 diffractometer using Cu Kα radiation (λ = 1.54058 Å), PW3020 generator and Bragg–Brentano geometry.

2.4.4. Mercury intrusion porosimetry (MIP)

Cubic samples of approximately 2 cm were analysed with a Micromeritics AutoPore IV 9500 series mercury intrusion porosimeter.

2.4.5. Environmental scanning electron microscopy (ESEM)

The microscopic morphology was observed by an Environmental scanning electron microscope Zeiss EVO 50 EP, equipped with an Oxford INCA 200 - Pentafet LZ4 spectrometer in secondary electrons mode.

2.4.6. Scanning laser profilometry

Wallettes profiles were recorded by means of a laser sensor with a 1.0 by 2.00 mm spot, a 40 μm resolution and a of 0.8% linearity, along a measurement range of 200 mm. The standard distance of the sensor from the surface was 100 mm with a +/−40 mm measurement range height. Two fixed sections for each wallette have been identified and used as reference positions for the measure-ments: one profile crossing the entire mortar joint along the longitudinal direction, and one profile crossing two joints and 3 courses of brick elements along the transversal direction. The damage index (mm^2 of area loss) at each testing stage is given by the area of the section defined by: (i) the reference initial profile of the wallette, and (ii) the profile recorded at the end of the cycle in the mortar joint region (which corresponds to the entire profile for the longitudinal section, and to two smaller areas of the joints crossed by the transversal section) (Fig. 1).

2.4.7. Data analysis

Data resulting from the characterisation and the damage evaluation were analysed by Principal Component Analysis (PCA). V-Parvus 2010 software was used for the calculation of principal component and data loadings.

3. Results and discussion

3.1. Materials characterisation

The complete characterisation of both the anhydrous materials and the hardened mortars are summarised in Table 1 [23]. The total anion content of the commercial products has been evaluated and can be considered under the detection limit in all specimens. It is therefore not reported. Porosity of the mortars has been evaluated using two different substrate conditions: a steel substrate representative of the microstructure of the cubic specimens [23] and a brick porous substrate providing a better simulation of the wallettes.

The porosity and pore size distribution results of the latter condition are reported in Table 1 and Fig. 2. It can be observed that the presence of the porous substrate generally results in a slight reduction of the total porosity values, due to the draining effect of the brick. This effect seems not to affect M4, which regardless to the moulding condition develops the highest total porosity. The most significant variation occurs with respect to the pore distribution rather than to the total porosity. In particular, mortar M2 shows a strong reduction of the median pore radius when prepared on a brick substrate, becoming comparable to M1. The same applies to B1 and B2, which both develop porosities smaller than 1 μm. The pore distribution of M1 (Fig. 2) remains narrowed around 0.03 μm with most of the pores laying below 0.05 μm, thus confirming the results of the steel moulded sample [23]. A rather similar curve is exhibited by M2, but having a wider distribution of pores all located below 1 μm. The two commercial binders display a similar and dispersed pore structure in a range going from the finest fraction up to 1 μm threshold. Moreover, a bimodal distribution can be identified for B1 with a secondary pore concentration centred around 0.4 μm. M3 and M4 have distinguished pore concentrations toward the coarser diameters. They are both characterised by narrow peaks at 1 μm; M4 then displays a constantly decreasing curve towards finer pore diameters, whereas M3 has a further wide pore distribution centred around 0.05 μm.

In Fig. 3, the percentage of pores below 0.1 μm and 0.01 μm respect to the total porosity is reported for each mortar according to the preparation condition. The two pore fractions have been selected because they are relevant with respect to the durability of these materials [36]. The 0.1 μm fraction is particularly sensitive to the change of the substrate, and all mortars show limited (M4) to high (B1) increase of the pore percentages when casted in the wallettes (on bricks). The variations within the finest fraction (below 0.01 μm) are less evident and can be considered negligible in most cases. The only significant increase of the pores percentage occurs in M2, whereas M4 shows a small reduction.

The capillary water absorption of the mortars has been evaluated according to UNI EN standard [37]. The results are reported

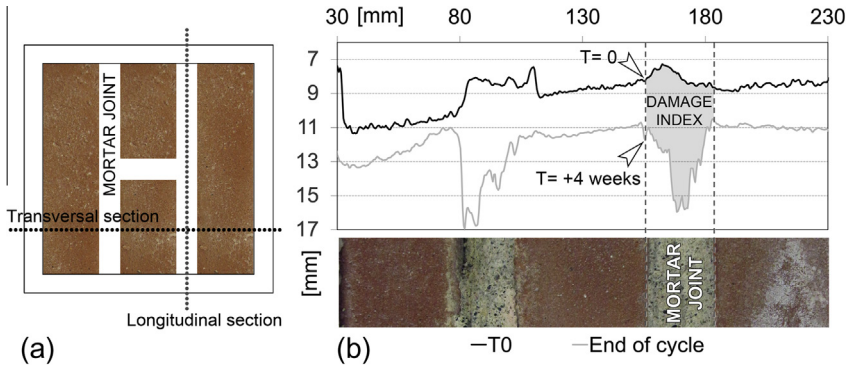

Fig. 1. Scheme of a wallette with indication of the two sections for the damage evaluation (a). Evaluation of the damage index (loss of area) through laser profilometry (b): area of the section defined by the reference initial profile of the wallette (T = 0) and the profile recorded at the end of the cycle in the mortar joint region (T = +4 weeks; transversal section).

Table 1
Summary of the main compositional, mechanical and microstructural features of the commercial ready mixed mortars and NHL commercial binders.

Sample	Anhydrous commercial products							Hardened mortars				
	Binder NHL class	XRD results						Compressive strength (MPa)	Steel substrate		Brick substrate	
		P	L	F	C	D	Q		Porosity (%)	Median pore radius (μm)	Porosity (%)	Median pore radius (μm)
M1	n.d.	++	–	+++	+	–	+++	9.57	30.37	0.05	27.60	0.03
M2	n.d.	–	++	+	+++	–	++	10.06	26.48	0.16	25.11	0.03
M3	3.5	–	++	–	+++	+	++	8.84	27.08	0.43	26.58	0.14
M4	5	–	+	–	++	++ +	+	4.39	34.26	0.66	34.21	0.48
B1	3.5	++ +	+++	–	+	–	++	4.70	22.59	0.27	19.25	0.06
B2	5	–	++	–	+++	++	++	7.38	21.42	0.20	19.63	0.07

+++ = dominantly present, ++ = present, + = traces, – = not detected.
P = portlandite, L = larnite, F = feldspar, C = calcite, D = dolomite, Q = quartz.

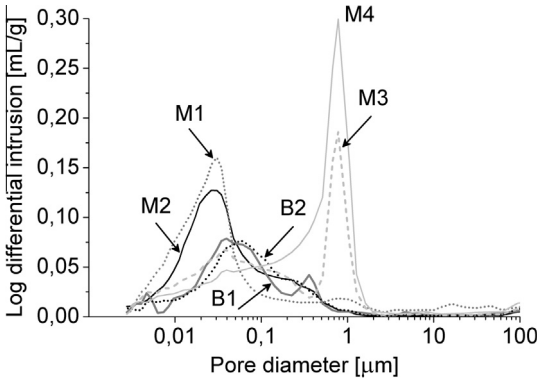

Fig. 2. Pore size distribution of hardened mortars prepared on porous substrates as measured by MIP.

in Fig. 4. M3, M4, B1 and B2 show a rapid and comparable absorption capability during the initial step of the test (1 h) with final absorption values ranging from 8000 g/m^2 (B1) to 12,000 g/m^2 (M4). B2 has a much lower final absorption value around 5000 g/m^2. The initial water absorption of M1 is slower than the previous ones and lead to a final value between those of B1 and M3. M2 greatly differs from all other specimens for its very slow and limited capillary water absorption capability. This unexpected trend cannot be only explained with the differences in the porosimetric features and it is most probably related to the presence of a water repellent agent in the initial composition. Generally such compounds are added in very low amount so that their identification by means of the traditional characterisation techniques cannot always be possible.

3.2. Durability to salt decay of cubic specimens

After seven week-cycles almost all specimens were damaged to various extents. The formation of efflorescences on the evaporation front was used to confirm the migration of the salt solution through the entire specimen. The two samples belonging to the commercial binders (B1 and B2) start showing superficial crystallization along the lateral edges of the upper surface since the first daily cycle, whereas all the other mortars develop superficial efflorescences during the second week-cycle. Crust-like formation becomes the prevailing crystallization pattern as the test proceeds. M2 shows a singular behaviour as it does not reveal any sign of crystallization on the upper evaporation surface for the entire test duration.

Visible damage is occurring during the third week-cycle in form of contour scaling of the evaporation front of mortar B2 and as limited scaling of the lateral edges and corners for mortar M1.

The photographic documentation of the damage evolution after 4 weeks is reported in Fig. 5. M1, M4, and B2 developed a thick and extensively fractured salt crust over a partially disaggregated mortar; M3 shows only an irregular powder-like crystallization and moderate scaling, while B1 is partly covered by a salt crust crossed by elongated fibrous-like crystals. In this last case, the crust is strongly attached to the substrate and the presence of few small flakes indicates a rather good state of conservation of the mortar. M2 appears totally unaltered.

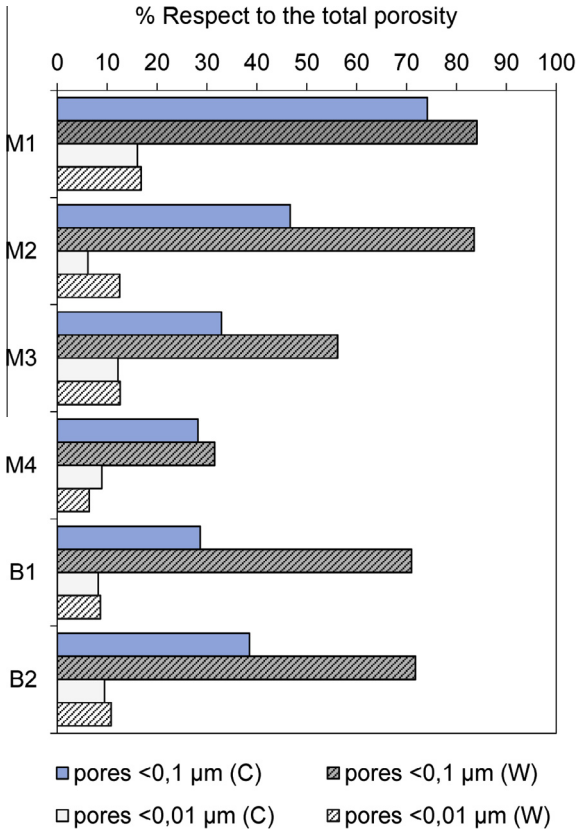

Fig. 3. Variations of the pores concentration (with respect to the % total porosity) of two selected dimensional fractions as a result of different preparation conditions: cubic specimen casted in steel mould (C), and wallettes (W).

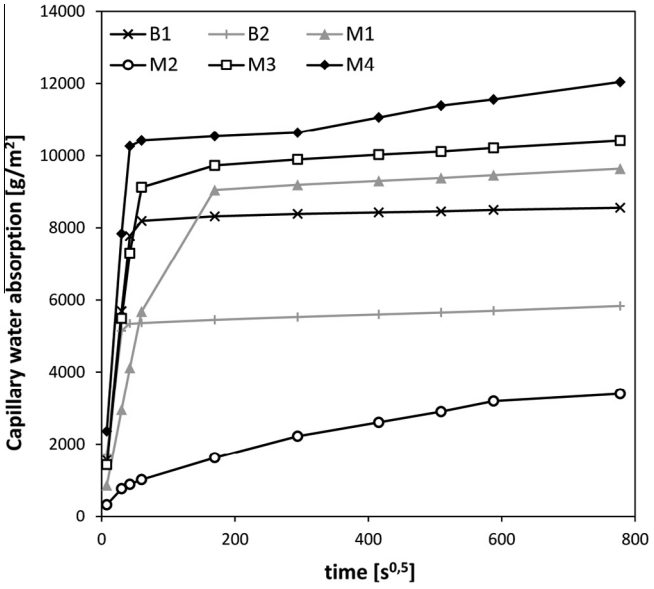

Fig. 4. Capillary water absorption of the mortars (cubic specimens).

At this stage of the testing, a closer observation of the surface of the most damaged specimens (M1, M4 and B2) allows to identify two main crystallization patterns: a salt crust embedding mortar's flakes with loose grains belonging to the aggregate fraction and a diffused network of elongated fibre-like crystals growing underneath (Fig. 6). These crystals develop just beneath the surface and tend to grow perpendicularly, up to a 5 mm length. The mechanical stress induced by the growing crystals is responsible for the progressive detachment and fracturing of the uppermost surface, according to a damage mechanism which has been reported for different types of substrates [38]. The crust appears quite stable both during the humid (daily cycles) and the drying stages (at the end of each weekly cycle), whereas the fibre-like crystals are no longer visible after the samples are dried. According to Flatt [29], the humid condition following imbibition promotes the precipitation of mirabilite (or a mix of mirabilite and thenardite), which can develop prismatic elongated crystals. As a result of the temperature increase during the drying phase (+40 °C), mirabilite rapidly dehydrates into smaller thenardite crystals.

The mass variation of the mortars is used for the evaluation of the damage. The results are reported in Fig. 7. The damage progression can be described according to the three stages approach proposed by Angeli et al. [39]: (i) salt uptake; (ii) mass variation as a result of the competition between salt uptake and mortar damage; (iii) predominant mortar damage.

Most of the salt accumulation due to capillary absorption of the salt solution takes place during the first stage, corresponding to weekly cycles I and II (Fig. 7). As a result, all specimens except M2 show mass increases due to salt uptake and start developing superficial crystallization with different patterns, as previously discussed, but no visible damage. Mortars show a different imbibition attitude (Fig. 8) which is mainly driven by the specific microstructural features of the different materials. The presence of a coarse porosity connected to smaller pores with a decreasing distribution towards the finest diameters [23] promotes rapid salt uptake of M3 since the very first cycle. The mass variation between the first and the second week of testing is limited and M3 finally show the highest salt uptake value. M1 and M4 have a rather comparable mass increase after two weeks, slightly over 4% with respect to the initial weight. Moreover M4 displays the most consistent variation between cycle I and cycle II. This can be related to presence of coarse pores and to its high total porosity, which provide space for salt accumulation. The two specimens prepared with commer-cial binders differ in terms of imbibition capacity despite their mutually comparable porosity values, being B1 more prone to absorb the solution (more than +3% mass increase) with respect to B2 (around +1.5% mass increase). The mass variation of M2 is very low, around 0.3%, and can be considered negligible. This peculiar behaviour of M2 sample is maintained during the entire duration of the test (Fig. 7) and the mass stability after 7 cycles confirms that a very limited amount of solution has been absorbed. This result is consistent with the capillary absorption test and the possible presence of a water repellent agent in the mortar. Moreover, under the compositional point of view, the presence of slag fragments within the binder fraction [23] can also contribute to enhance the differential response to salt weathering with respect to the other tested materials [40].

During the second stage of damage evolution limited mass variations of the specimens are associated to the first appearance of visible deterioration patterns. This stage can be considered as the final one for B1 and M3, whose weights remain well above the initial ones during the entire test. For both mortars the damage is therefore limited and the related loss of material is quantitatively competitive with the weight increase due to salt uptake. Second stage of damage can also be identified for mortars M1 and M4 during cycle III, in which superficial crust formation still represents the main decay pattern.

Third stage of damage evolution can be observed for M1 and M4 starting from cycle IV. The damage prevails over salt accumulation and the related mass variation shows a not linear trend: damage increases as the superficial crust and the underlying disaggregated

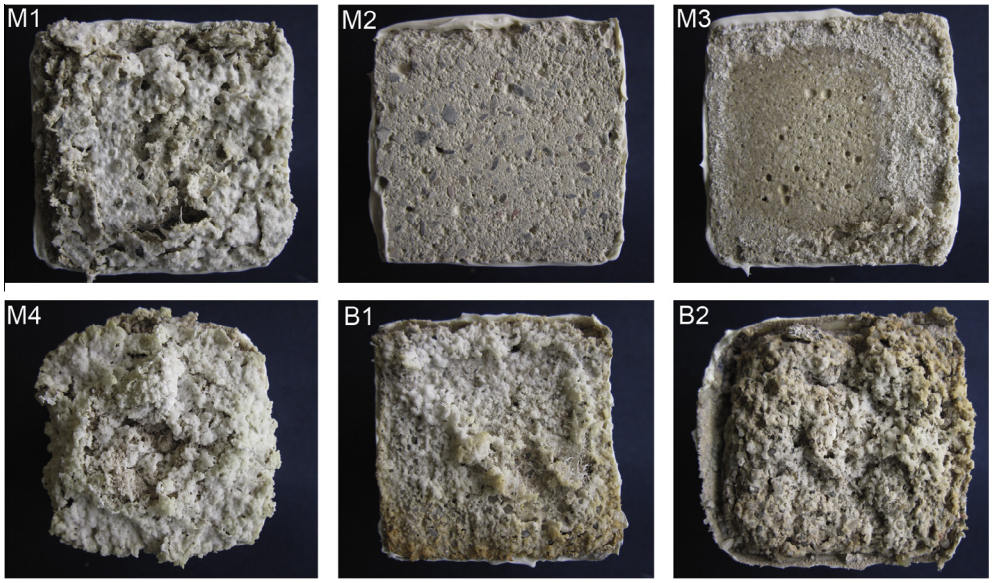

Fig. 5. Photographic documentation of the damage evolution and decay patterns of cubic specimens at the end of cycle IV of testing (side of the specimens = 4 cm).

Fig. 6. Stereomicroscopic documentation of a recurrent decay pattern at the evaporation surface of the specimens: thin elongated fibrous crystals of sodium sulphate growing within a partly disaggregated substrate and detaching the superficial salt crust.

material detach (cycles IV and VII); damage slows down as a new salt crust forms (cycles V and VI). The last crystallization cycle seems to be the most damaging. The final damage extent is particularly severe for M1 and can be quantified as 35% loss of the initial weight. No transition through second stage of damage evolution can be observed for mortar B2. The third stage begins right after the initial salt accumulation (cycles I and II), as the mass decrease induced by the loss of materials overcomes the salt uptake. The damage then proceeds almost linearly until a final result comparable to that of M4.

According to the final mass variation, the durability to salt crystallization can be divided into four categories: (i) *no damage*, M2; (ii) *low damage*, M3 and B1; (iii) *moderate damage*, M4 and B2;(iv) *high damage*, M1. The photographic documentation of the specimen at the end of the test is reported in Fig. 9.

ESEM observation of the upper surface of M1 shows the presence of aggregates of well-formed prismatic sodium sulphate crystals (Fig. 10a) with an average dimension up to 20 μm. The morphology and size of the crystals are similar to those reported in the case of mirabilite precipitation [24,41]. Crystallization occurring just beneath the surface concentrates the mechanical stress within the most external layer of the material, and is responsible for the contour scaling and massive crust detachment observed during the last cycle.

The ESEM observation of specimen M3 at the end of the test shows a different situation respect to M1 and suggests that the mortar's matrix has been more capable to sustain crystallization with less damage; sodium sulphate crystals are present in smaller aggregates and they have mostly formed within the pores and the discontinuities of the material (Fig. 10b). No fractures of the matrix

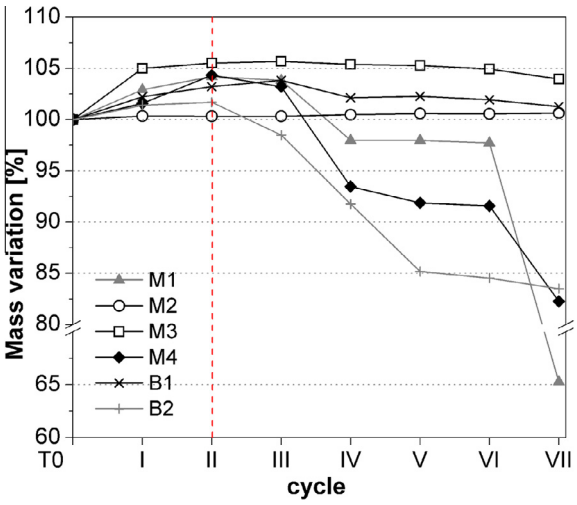

Fig. 7. Damage evolution as mass variation of the specimens versus number of testing cycles.

can be observed. As far as these two rather different situations (low/high damage) are concerned, it has to be noted that a direct correlation between the damage extent and the compressive strength values cannot be clearly identified, as both mortars have a comparable mechanical behaviour. A similar consideration can be drawn in case of B1, whose final damage level is the same of M3 despite a significantly lower mechanical resistance. Considering the overall heterogeneity of the features of the mor-tars, and according to previous studies which highlight the rele-vance of the pore distribution as a key factor for salt susceptibility [42–44], the poor performance of mortar M1 can be mainly related to the concentration of pores having smaller diameters with respect to the other tested materials [23]. The high supersaturation ratio developed in such condition increases the possibility that high crystallization pressures are generated beneath the evaporation surface [43], thus intensifying the mechanical stress and the damage. Moreover, the availability of large porosity connected to smaller pores, as in the case of M1, can provide a reservoir of saline solution able to sustain prolonged crystallization [44].

3.3. Durability to salt decay of wallettes

Shortly after the preliminary imbibition, all specimens show diffused superficial crystallization: efflorescences over the mortar joints and bricks in forms of elongated fibrous crystals and powdered material. Small salt plaques preluding to crust formation are observed in M4, B1 and B2.

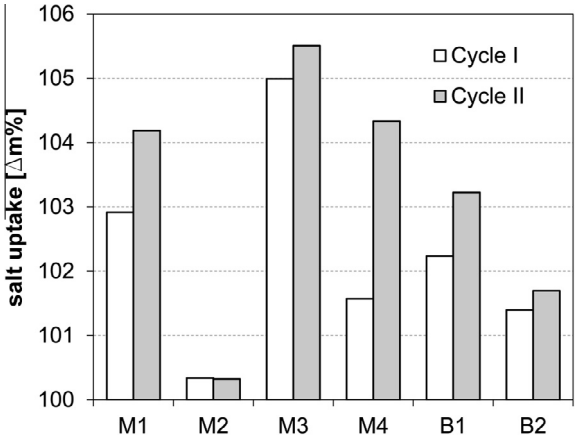

Fig. 8. Salt uptake of the specimens during the two initial cycles of testing (% mass variation with respect to normalised initial weight).

Starting from the end of cycle I, damage occurs firstly at the expenses of the bricks. All specimens show blistering, partial delamination, detachment and loss of adhesion of some brick elements as a result of the growing of elongated prismatic crystal just beneath the surface or at the brick/mortar interface. As far as the mortar joints are concerned, diffused whitening is observed as a result of the salt migration and crystallization, as well as limited disintegration of the matrix (B1 and B2) and minor scaling (M3). After the first re-wetting of the system, the superficial fibrous-like crystallization initially formed is dissolved and substituted by a thick salt crust, in some cases (B1 and B2, in particular) strongly adherent to the substrate and hardly removable.

In Fig. 11 is reported the damage progression of wallettes M1 and M3 after laser profilometry monitoring. These two cases have been selected being representative of rather different durability results and showing distinct damage evolutions.

Salt migration and accumulation just beneath the surface of M1 during the first cycle induces mechanical stresses on the outer layer of the wallette. As a result, the central brick element shows a rising of the profile due to blistering, whereas the two lateral bricks demonstrate a more advanced progression of the same decay pattern with loss of material. Blistering followed by brick delamination and detachment is triggered by the mechanical actions of crypto-efflorescences. Diffused elongated prismatic crystals (with an average length up to 5 mm) develop within the outer portion of the substrates and grow perpendicularly towards the evaporation front. The profile evolution highlights that most of the damage to the bricks occurs between cycle I and III, at early stages of the testing. The loss of material then proceeds with a much slower rate. During the same early stages, the actual damage of the mortars is limited, and the irregular rise of the mortar pro-files (both along longitudinal and transversal direction) depends on the formation of the adherent salt crust previously discussed. Most of the damage to the mortar is developed during the subsequent stage (corresponding to cycles IV–VI). The loss of material is detected along the transversal direction of the wallette, due to the detachment of thick scales and to mortar disintegration. The damage monitored along the longitudinal direction is consistent with the transversal one. The first two profiles (cycles I–III) show limited and irregular damaging particularly located near the external borders. These areas demonstrate to be more susceptible to salt weathering, as they suffer the most intense loss of material. Cracks formation and scaling are here particularly effective because of the edges of the joint, which provide supplemental evaporation fronts and enhance further crystallization. During the last crystallization cycle the loss of material is particularly concentrated in the central part of the joint. As for the transversal joints, the final damage extent can be estimated in 12 mm-depth loss of material, while along the longitudinal one is slightly higher around 20 mm-depth.

The damage evolution of M3 shows a much more homogeneous trend with respect to M1, and the loss of material from the joints is similar to the one from the bricks as for extent and deterioration rate. Similarly to M1, the initial formation of the salt crust determines some local rising of the profile during cycle I. Both profiles highlight an increased surface roughness mostly affecting the mortar (longitudinal profile) and one of the brick. Most of the damage occurs during cycle III and in forms of scaling of the mortar and brick delamination. The damage progression during the remains of the test is extremely limited so that no significant variations occur to the mortar between cycle VIII and the final one.

According to the loss of material trend reported in Fig. 12 and to the monitoring of the deterioration patterns, the following remarks can be drawn with respect to the salt decay attitude:

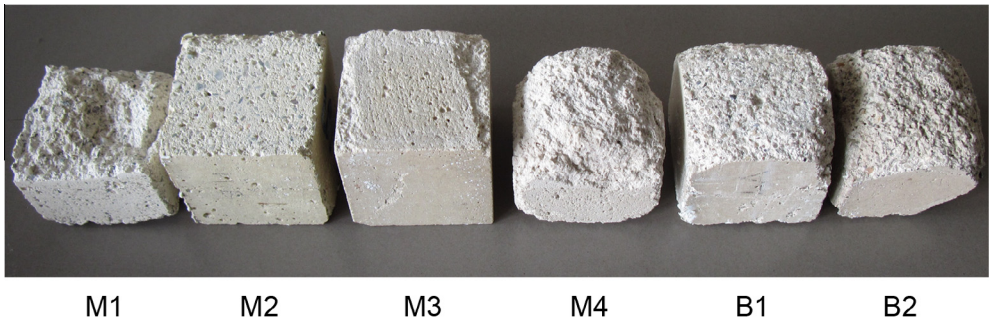

Fig. 9. Photographic documentation of the decay extent at the end of the test.

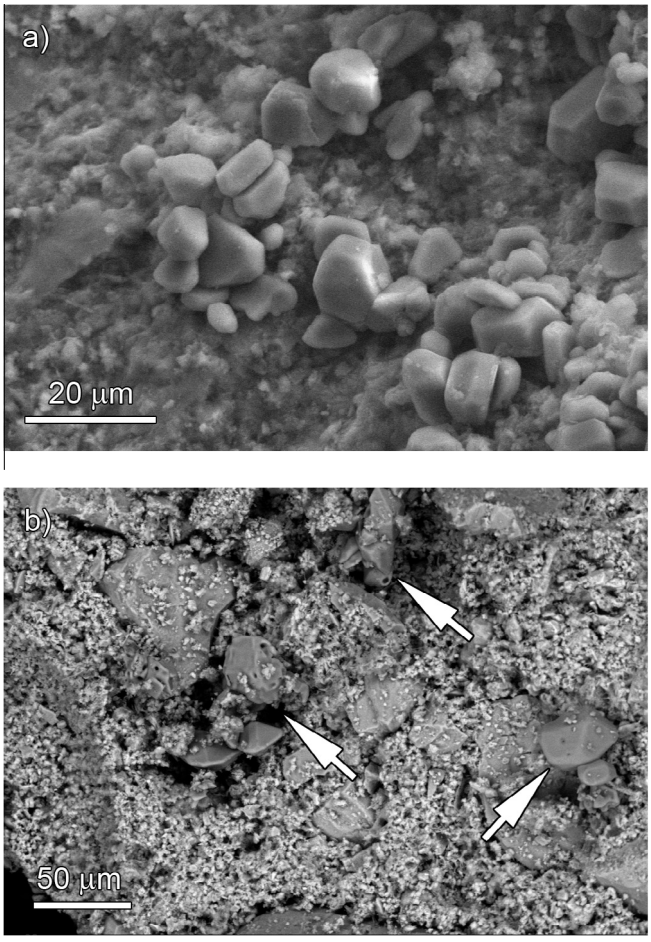

Fig. 10. ESEM observation of the specimens surface at the end of the test. Arrows indicated aggregates of sodium sulphates at the interface of a detached scale of mortar M1 (a), and crystallization within the pore space and discontinuities of mortar M3 (b).

- M3, M4 and B1 demonstrate a low and rather constant damage attitude resulting in minor scaling and disintegration of the matrix. The apparent material increase of B1 during cycle II (visible on both profile directions) corresponds to salt crust formation as previously discussed and it is not damage-related.
- M2 and B2 show a constant loss of material, generally more intense than the previous one. The two mortars demonstrate a similar damage trend especially if the longitudinal direction is considered. Both mortars develop a particular deterioration pattern: mortar disintegration tends to concentrate in the central area of the joints and it is less effective along the border, so that the loss of material is irregularly distributed.
- M1 provides low durability result. Until cycle III of the test, the behaviour of the mortar is still comparable to all the other examined. Once this threshold is passed, the mortar resistance drops and any further dissolution/crystallization cycle increases the damage. Moreover, during the last cycles mortar scaling is promoted as a result of the formation of wide cracks in a deeply disaggregated mortar's matrix.

The behaviour to salt crystallization of the mortars prepared as wallettes can be defined as: (i) *low damage*, M3, M4 and B1; (ii) *moderate damage*, M2 and B2; (iii) *high damage*, M1.

The salt resistance of the wallettes are generally in accordance with those of the cubic specimens. Despite the different crystallization procedure and taking into account the diverse methodology for damage quantification, which do not allow for a direct compar-ison between the two set of results, M1, M3, B1 and B2 maintain a similar final level of damage in both testing conditions. M1, in particular, is confirmed to display the lower durability result. The performance of M4 under the wallette condition seems to slightly increase and is associated to a mild reduction of the pores concentration towards the finest fraction (Fig. 3). It is worth noting that the wallettes actually represents a far more complex substrate with respect to the cubic mortar specimens due to the interaction of the porous bricks. Beside the variations induced in the mortar porosity (Fig. 2), the presence of the bricks and the specific design of the specimen influence the migration of the saline solution. The reduction of the durability of M2 has to be interpreted taking into account such aspects. The very low saline solution absorption observed for the mortar specimen in this case can be partly impaired by the presence of the surrounding bricks. These can act as a reservoir of salt which are available for a slow but more prolonged migration towards the low-absorbing mortar.

3.4. Correlation between mortars characteristics and salt decay susceptibility

Given the heterogeneity of the tested materials, the correlation between the mortars characteristics and the durability to salt decay was studied by means of PCA. All the characterisation fea-tures were initially evaluated (22 variables). The preliminary results allowed to identify the most significant data and to reduce the final dataset to 12 variables with no loss of information. The salt decay susceptibility was described by the salt uptake and the mass variations for the cubic specimens, and by the loss of material along the transversal and the longitudinal profiles for the wallettes. Three principal component were considered which accounted for 86.8% (cubic specimens) and 94.6% (wallettes) of the total variance. The loading plot of the cubic specimens resulting from PCA is reported in Fig. 13a. The loading vectors are representative of the original variables. The length of the vector is proportional to its

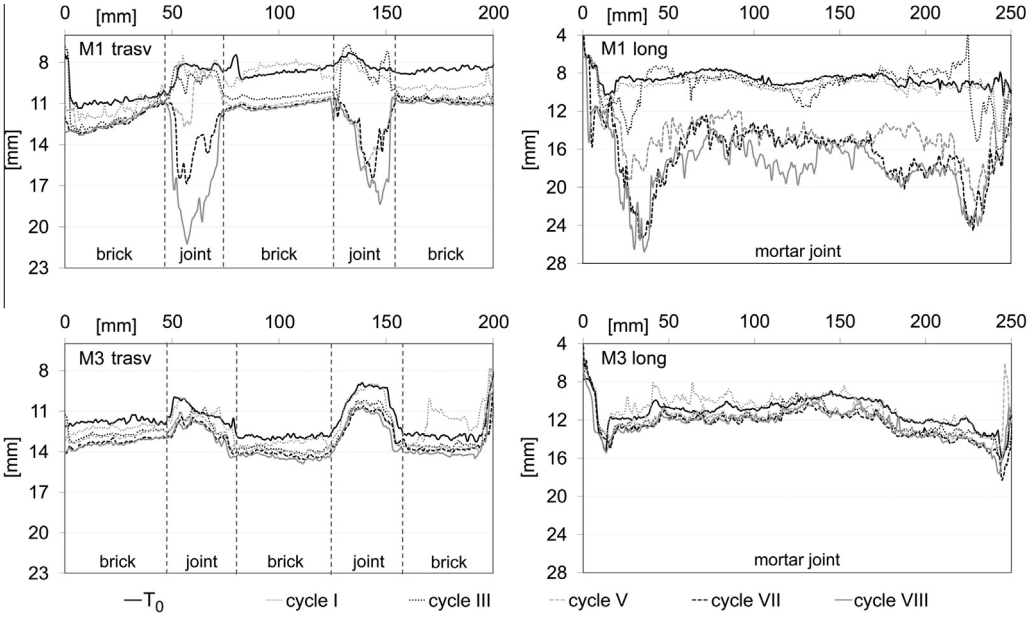

Fig. 11. Damage evaluation of mortars M1 and M3 as measured by laser profilometry along the transversal (trasv) and longitudinal (long) direction of the wallettes.

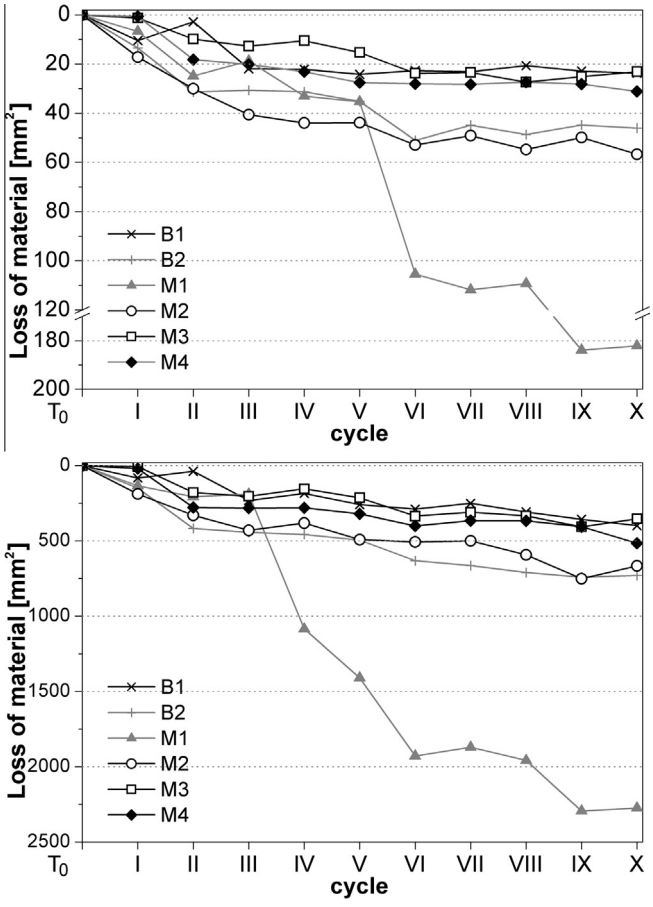

Fig. 12. Damage evolution of the wallettes according to the damage index (loss of area) measured along the transversal direction (above) and the longitudinal one (below).

significance with respect to the considered principal component. The angle formed by each couples of variables is related to their correlation: as the angle grows the correlation become less significant. PC1 accounts for 45.3% of the total variance and it is mainly linked to the type of aggregates, the pore percentages in the two fine fractions (<0.1 μm and <0.01 μm), the content of hydraulic compounds (di-calcium silicate – larnite) and the mass variation. PC2 accounts for 28.3% of the total variance and it is mainly linked to the microstructural features (total porosity, median pore radius and bulk density) and the salt uptake. As far as the mechanical behaviour is concerned, the results of the PCA confirmed that a correlation between the damage and the mechanical resistance measured as uniaxial compressive strength (σC) cannot be clearly identified. The compressive strength is positively correlated to the siliceous aggregate (Si agg, in Fig. 13) and portlandite content (P) and has a negative correlation with the amount of carbonatic aggregate (Ca agg). The salt uptake of the mortars (salt uptake %) is highly correlated to both porosity (positive correlation) and bulk density (negative correlation), whereas the median pore radius (Med pore rad) does not significantly affect neither the quantity of salt solution absorbed during the early stage of testing nor the final damage (Mass var %). On the contrary, the percentage of pores belonging to the finest fraction (Por < 0.01 μm) is highly correlated to the mass variation. The loading plot of PCA for the wallettes is reported in Fig. 13b. The correlations between the compressive strength and the aggregate composition, and the one linking the porosity to the bulk density (results of the salt uptake are not available for wallettes) also apply. Again, the uniaxial compressive strength cannot be directly correlated to the damage. PC1 in this case accounts for 52.3% of the total variance and it is mainly linked to the siliceous aggregate, the finest porosimetric fraction and the damage. PC2 accounts for 30.2% of the total variance and it is mainly linked to the total porosity, bulk density and content of hydraulic compounds. It is worth noting that the longitudinal and transverse damage show a very high correlation (L damage and T damage, in Fig. 13b), indicating that both variables are suit-able for the salt decay evaluation. Damage and pore percentage <0.01 μm remain correlated but to a minor extent, as a result of the influence of the pore system of the bricks.

4. Conclusions

The selected commercial ready-mixed mortars and NHL-based binders are specifically designed for the intervention on the built

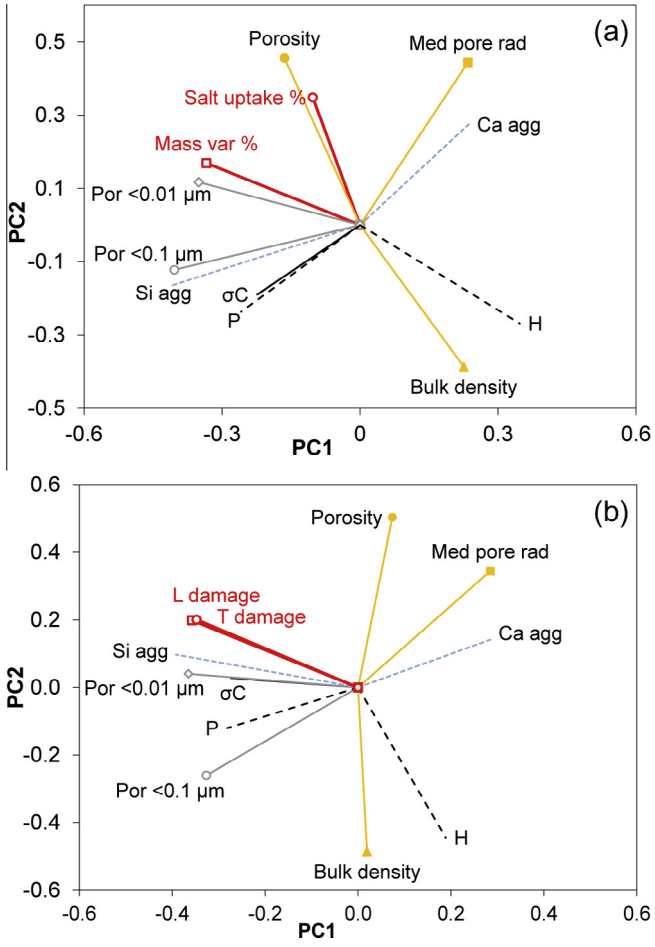

Fig. 13. Loading plots from PCA of selected characterisation and damage data of cubic specimens (a) and wallettes (b). Med pore rad = median pore radius; H = larnite content; P = portlandite; Ca agg = carbonatic aggregate; Si agg = siliceous aggregate; σC = compressive strength; Por < 0.1 μm = percentage of pores below 0.1 μm; Por < 0.01 μm = percentage of pores below 0.01 μm; Mass var = mass variation; L damage = damage along the longitudinal direction; T damage = damage along the transverse direction.

heritage. This paper explored the resistance of these materials to the salt crystallization damage. The examined materials behave very differently with respect to sodium sulphate as for damage evolution, decay extent and deterioration patterns. Sodium sulphate crystallization generally induces loss of material in form of granular disintegration and contour scaling of the mortar. In the wallettes severe delamination of the bricks has been observed as well.

The adopted testing procedures have been able to differentiate mortars according to their different salt resistance and allowed to identify the less durable material: M1 proved to be not compatible under the salt susceptibility point of view, due to the rapid damage evolution and to the consequent early stage failure. Nevertheless, a reliable prediction of the durability to salt decay of ready-mixed mortars (which are highly heterogeneous materials) on the basis of their compositional, mechanical and microstructural features still represents a challenging task.

PCA analysis has been able to identify a direct correlation between the considered damage parameters and a specific microstructural feature. The most relevant variable influencing the damage is the pore size distribution. In particular, a high amount of pores concentrated in the range of fine diameters (below 0.01 μm) is generally associated to major damage of the mortar tested on cubic specimens and, to a less extent, also on wallettes. This can be therefore considered a risk factor in the salt decay susceptibility evaluation. On the other hand, the direct influence of the compositional and mechanical (uniaxial compressive strength) properties on salt resistance cannot be still thoroughly understood.

The decision-making process for the selection of the restoration materials can take advantage of a complete testing procedure and cannot be based on the knowledge of some single "spot" parameters, such as a rather good compressive strength.

Acknowledgment

The authors wish to thank Professor L. Binda for the important suggestions provided during the experimental phase and the elaboration of the data.

References

[1] S. Siegesmund, R. Snethlage, Stone in Architecture. Properties, Durability, Springer, Berlin, Heidelberg, 2011.
[2] C. Sabbioni, A. Bonazza, G. Zappia, Damage on hydraulic mortars: the Venice Arsenal, J. Cult. Herit. 3 (1) (2002) 83–88.
[3] C. Cardell, F. Delalieux, K. Roumpopoulos, A. Moropoulou, F. Auger, R. Van Grieken, Salt-induced decay in calcareous stone monuments and buildings in a marine environment in SW France, Constr. Build. Mater. 17 (3) (2003) 165–179.
[4] B. Lubelli, R.P.J. van Hees, C.W.P. Groot, Investigation on the behaviour of a restoration plaster applied on heavy salt loaded masonry, Constr. Build. Mater. 20 (9) (2006) 691–699.
[5] H. Siedel, E.V. Plehwe-Leisen, H. Leisen, Salt load and deterioration of sandstone at the temple of Angkor Wat, Cambodia, in: J.W. Lukaszewicz, P. Niemcewicz (Eds.), International Congress on Deterioration and Conservation of Stone, Nicolaus Copernicus University, Torun, Poland, 2008, pp. 267–274.
[6] D. Gulotta, M. Bertoldi, S. Bortolotto, P. Fermo, A. Piazzalunga, L. Toniolo, The Angera stone: a challenging conservation issue in the polluted environment of Milan (Italy), Earth Sci. Environ. (2012) 1085–1094.
[7] A. Charola, Salts in the deterioration of porous material: an overview, J. Am. Inst. Conserv. 39 (3) (2000) 327–343.
[8] E. Doehne, Salt weathering: a selective review, in: S. Siegesmund, T.N. Weiss, A. Vollbrecht (Eds.), Natural Stone, Weathering Phenomena, Conservation Strategies and Case Studies, Geological Society, 2002, pp. 51–64.
[9] M. Steiger, S. Siegesmund, Special issue on salt decay, Environ. Geol. 52 (2) (2007) 185–186.
[10] E.F. Doehne, C.A. Price, Institute TGC, Stone conservation: an overview of current research, J. Paul Getty Mus. Publ. (2011).
[11] W. Kloppmann, P. Bromblet, J.M. Vallet, V. Vergès-Belmin, O. Rolland, C. Guerrot, et al., Building materials as intrinsic sources of sulphate: a hidden face of salt weathering of historical monuments investigated through multi-isotope tracing (B, O, S), Sci. Total Environ. 409 (9) (2011) 1658–1669.
[12] P. Lopez-Arce, J. Garcia-Guinea, D. Benavente, L. Tormo, E. Doehne, Deterioration of dolostone by magnesium sulphate salt: an example of incompatible building materials at Bonaval Monastery, Spain, Constr. Build. Mater. 23 (2) (2009) 846–855.
[13] H. De Clercq, M. Jovanović, K. Linnow, M. Steiger, Performance of limestones laden with mixed salt solutions of Na_2SO_4–$NaNO_3$ and Na_2SO_4–K_2SO_4, Earth Sci. Environ. (2012) 1–11.
[14] K. Zehnder, Long-term monitoring of wall paintings affected by soluble salts, Environ. Geol. 52 (2) (2007) 353–367.
[15] A. Sawdy, A. Heritage, L. Pel, A review of salt transport in porous media, assessment methods and salt reduction treatments, in: International Congress Salt Weathering on Buildings and Stone Sculptures, Department of Civil Engineering, Technical University of Denmark, Copenhagen, 2008, pp. 1–27.
[16] Characterization of old mortars with respect to their repair, in: C. Groot, G. Ashall, J.J. Hughes (Eds.), Final Report of RILEM TC 167-COM, 2004.
[17] K. Van Balen, I. Papayianni, R. Van Hees, L. Binda, A. Waldum, Introduction to requirements for and functions and properties of repair mortars, Mater. Struct. 38 (8) (2005) 781–785.
[18] Rilem Technical Committee T-RRepair mortars for historic masonry. Testing of hardened mortars, a process of questioning and interpreting, Mater. Struct. 42 (2009) 853–865.
[19] J.D. Rodrigues, A. Grossi, Indicators and ratings for the compatibility assessment of conservation actions, J. Cult. Herit. 8 (1) (2007) 32–43.
[20] L. Schueremans, Ö. Cizer, E. Janssens, G. Serré, K.V. Balen, Characterization of repair mortars for the assessment of their compatibility in restoration projects: research and practice, Constr. Build. Mater. 25 (12) (2011) 4338–4350.
[21] I. Papayianni, V. Pachta, M. Stefanidou, Analysis of ancient mortars and design of compatible repair mortars: the case study of Odeion of the archaeological site of Dion, Constr. Build. Mater. 40 (2013) 84–92.

[22] A. Isebaert, L. Van Parys, V. Cnudde, Composition and compatibility requirements of mineral repair mortars for stone – a review, Constr. Build. Mater. 59 (2014) 39–50.
[23] D. Gulotta, S. Goidanich, C. Tedeschi, T.G. Nijland, L. Toniolo, Commercial NHL-containing mortars for the preservation of historical architecture. Part 1: compositional and mechanical characterisation, Constr. Build. Mater. 38 (2013) 31–42.
[24] A. Arizzi, H. Viles, G. Cultrone, Experimental testing of the durability of lime-based mortars used for rendering historic buildings, Constr. Build. Mater. 28 (1) (2012) 807–818.
[25] P. Faria Rodrigues, Resistance to salts of lime and pozzolan mortars, in: International RILEM Workshop on Repair Mortars for Historic Masonry, Delft, The Netherlands, 2005, 99–110.
[26] TC Rilem 127-MSTests for masonry materials and structures, Mater. Struct. 31 (1998) 2–19.
[27] A. Hamilton, C. Hall, L. Pel, Sodium sulfate heptahydrate: direct observation of crystallization in a porous material, J. Phys. D Appl. Phys. 41 (21) (2008) 1–5.
[28] R.M. Espinosa-Marzal, G.W. Scherer, Advances in understanding damage by salt crystallization, Acc. Chem. Res. 43 (6) (2010) 897–905.
[29] R.J. Flatt, Salt damage in porous materials: how high supersaturations are generated, J. Cryst. Growth 242 (3–4) (2002) 435–454.
[30] C. Rodriguez-Navarro, E. Doehne, E. Sebastian, How does sodium sulfate crystallize? Implications for the decay and testing of building materials, Cem. Concr. Res. 30 (10) (2000) 1527–1534.
[31] T.A. Saidov, R.M. Espinosa-Marzal, L. Pel, G.W. Scherer, Nucleation of sodium sulfate heptahydrate on mineral substrates studied by nuclear magnetic resonance, J. Cryst. Growth 338 (1) (2012) 166–169.
[32] A. Moropoulou, K. Polikreti, A. Bakolas, P. Michailidis, Correlation of physicochemical and mechanical properties of historical mortars and classification by multivariate statistics, Cem. Concr. Res. 33 (6) (2003) 891–898.
[33] A. Moropoulou, K. Polikreti, Principal component analysis in monument conservation: three application examples, J. Cult. Herit. 10 (1) (2009) 73–81.
[34] UNI-EN 459-1, Building Lime – Definitions, Specification and Conformity Criteria, 2010.
[35] UNI-EN 196-1, Methods of Testing Cement – Part 1: Determination of Strength, 2005.
[36] P. Theoulakis, A. Moropoulou, Microstructural and mechanical parameters determining the susceptibility of porous building stones to salt decay, Constr. Build. Mater. 11 (1) (1997) 65–71.
[37] UNI-EN 1925, Natural Stone Test Methods. Determination of Water Absorption Coefficient by Capillarity, 2010.
[38] E. Ruiz-Agudo, F. Mees, P. Jacobs, C. Rodriguez-Navarro, The role of saline solution properties on porous limestone salt weathering by magnesium and sodium sulfates, Environ. Geol. 52 (2) (2007) 269–281.
[39] M. Angeli, J.-P. Bigas, D. Benavente, B. Menéndez, R. Hébert, C. David, Salt crystallization in pores: quantification and estimation of damage, Environ. Geol. 52 (2) (2007) 205–213.
[40] T. Cerulli, C. Pistolesi, C. Maltese, D. Salvioni, Durability of traditional plasters with respect to blast furnace slag-based plaster, Cem. Concr. Res. 33 (9) (2003) 1375–1383.
[41] C. Rodriguez-Navarro, E. Doehne, E. Sebastian, Influencing crystallization damage in porous materials through the use of surfactants: experimental results using sodium dodecyl sulfate and cetyldimethylbenzylammonium chloride, Langmuir 16 (3) (1999) 947–954.
[42] D. Benavente, M.A.G. del Cura, J. García-Guinea, S. Sánchez-Moral, S. Ordóñez, Role of pore structure in salt crystallisation in unsaturated porous stone, J. Cryst. Growth 260 (3–4) (2004) 532–544.
[43] G.W. Scherer, Crystallization in pores, Cem. Concr. Res. 29 (8) (1999) 1347–1358.
[44] C. Rodriguez-Navarro, E. Doehne, Salt weathering: influence of evaporation rate, supersaturation and crystallization pattern, Earth Surf. Proc. Land. 24 (3) (1999) 191–209.